CHEMISTRY OF MATERIALS

Article

pubs.acs.org/cm

Stable Green Electroluminescence from an Iridium Tris-Heteroleptic Ionic Complex

Daniel Tordera,[†] Manuel Delgado,[†] Enrique Ortí,[†] Henk J. Bolink,*[,†] Julien Frey,[‡] Md. Khaja Nazeeruddin,[‡] and Etienne Baranoff*[,‡,§]

[†]Instituto de Ciencia Molecular, Universidad de Valencia, ES-46980 Paterna (Valencia), Spain

[‡]Laboratory of Photonics and Interfaces, Institute of Chemical Sciences and Engineering, École Polytechnique Fédérale de Lausanne, CH-1015 Lausanne, Switzerland

[§]School of Chemistry, University of Birmingham, Edgbaston, B15 2TT, England

Supporting Information

ABSTRACT: An ionic tris-heteroleptic iridium complex gives green light-emitting electrochemical cells (LECs) with unprecedented performances for this part of the visible spectrum. The devices are very bright (>1000 cd m^{-2}), efficient (~3%), and stable (>55 h). The novel complex is prepared using a new and efficient synthetic procedure. We show that there is a mixed orbital formation originating from the two different orthometalating ligands resulting in photophysical properties that lie between those of its two bis-heteroleptic analogs. Therefore, tris-heteroleptic complexes provide new avenues for fine-tunning the emission properties and to bridge gaps between a series of bis-heteroleptic complexes.

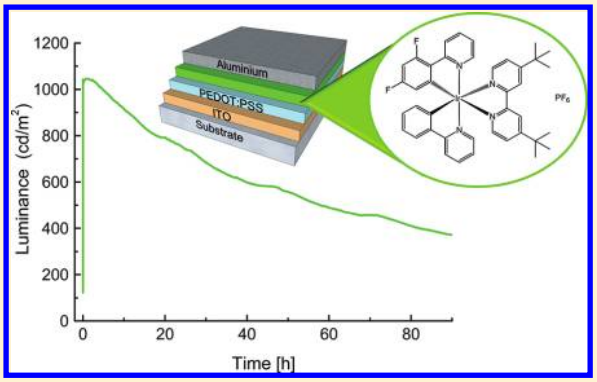

KEYWORDS: *light-emitting electrochemical cell, green electroluminescence, iridium complex, tris-heteroleptic complex*

INTRODUCTION

Light-emitting electrochemical cells (LECs) are single-layer electroluminescent devices consisting of a luminescent material in an ionic environment.[1−5] The luminescent material is either a conjugated light-emitting polymer or an ionic transition-metal complex (iTMC), leading to polymer-LECs (PLECs) or iTMC-LECs, respectively. The main characteristic of these devices is their insensitivity to the work function of the electrodes employed.[6,7] Therefore, in contrast to organic light-emitting diodes (OLEDs), air-stable electrodes, such as gold, silver, or aluminum, can be used, and their encapsulation does not have to be as rigorous as that with OLEDs. These characteristics make iTMC-LECs the simplest type of electroluminescent device.[8] A large number of iTMCs have been evaluated in LECs (most recently, using examples with iridium(III) as the metal core).[9−18] In many iridium(III)-based iTMCs (Ir-iTMCs), the highest-occupied molecular orbital (HOMO) and the lowest-unoccupied molecular orbital (LUMO) are localized on different parts of the complex, with the HOMO frequently residing on the cyclometalating C^N ligands and the Ir ion and the LUMO often lying on the neutral N^N ligand. Hence, one can change the energy of the HOMO and LUMO independently by selecting proper C^N and N^N ligands or by changing the substitution pattern of the ligands. This has indeed led to a large number of complexes emitting in most parts of the visible spectrum. However, the majority emit in the blue, yellow, and orange regions, with a few examples of pure green[12,19−23] and red emission.[20,24−26] Furthermore, the synthetic method predominantly used to make these Ir-iTMCs employs a μ-dichloro-bridged iridium dimer, $[Ir(C^N)_2(\mu\text{-}Cl)]_2$, containing the selected C^N ligands. In a second step, the dimer is reacted with the N^N ligand leading to the $[Ir(C^N)_2(N^N)]^+$ cation formation. Following this route, the final complex contains two identical C^N ligands, which reduces the possibility to fine-tune the photophysical properties of the complex.

Here, we present the synthesis (in high yields and purity) of a very efficient, pure green-light-emitting Ir-iTMC containing two different C^N ligands (2-phenylpyridine (ppy) and 2-(2,4-difluorophenyl)pyridine (diFppy)) and one N^N ligand (4,4′-di-*tert*-butyl-2,2′-bipyridine) (dtb-bpy)). LECs based on this tris-heteroleptic Ir-iTMC, $[Ir(ppy)(diFppy)(dtb\text{-}bpy)][PF_6]$ (**2**), show unprecedented performances for this part of the visible spectrum. The devices are very bright (>1000 cd m^{-2}), efficient (~3%), and stable (>55 h). The phosphorescence maximum of **2** lies between those of the corresponding bis-heteroleptic complexes $[Ir(ppy)_2(dtb\text{-}bpy)][PF_6]$ (**3**)[9] and $[Ir(diFppy)_2(dtb\text{-}bpy)][PF_6]$ (**4**).[27] Using density functional theory (DFT) calculations, it is shown that the HOMO, although distributed over both the diFppy and the ppy C^N ligands, is more localized on the less-electronegative ppy ligand.

Received: February 22, 2012
Published: April 23, 2012

   dx.doi.org/10.1021/cm3011716 | *Chem. Mater.* 2012, 24, 1896−1903

Coinciding with this, calculations show that the ppy ligand contributes in a greater extent to the emitting lowest-energy triplet state.

EXPERIMENTAL SECTION

Materials and General Considerations. All materials and solvents were of reagent quality and used as received. 4,4′-Di-*tert*-butyl-2,2′-bipyridine was purchased from Fluka, and complex **1** was prepared as previously reported.[28] ^{1}H NMR spectra were recorded using a Bruker AV 400 MHz spectrometer. Chemical shifts δ (in ppm) are referenced to residual solvent peaks. Coupling constants are expressed in units of hertz (Hz). High-resolution mass spectroscopy (HRMS) analysis and elemental analysis have been performed by the Service d'Analyse of EPFL. UV−visible spectra were recorded in a 1-cm-path-length quartz cell on a Hewlett−Packard Model 8453 spectrophotometer. The quantum yields were determined using fluorescein (10^{-5} M in 0.1 M NaOH; air-equilibrated; Φ_{PL} = 0.93) as standard.[29] Excited-state lifetimes were measured using a FL-1061PC TCSPC and 406 nm Nanoled as excitation source. Solutions were degassed by bubbling argon softly for 30 min. Voltammetric measurements employed a PC controlled AutoLab PSTAT10 electrochemical workstation and were carried out in an argon-filled glovebox, oxygen, and water (<5 ppm). All experiments were realized using 0.1 M $TBAPF_6$ in anhydrous acetonitrile (MeCN) as the electrolyte, using a set of carbon glassy, and two Pt wires (used as the working electrode, the counter electrode, and the reference electrode, respectively). Ferrocene was used as internal standard. A scan rate of 100 mV s^{-1} has been applied. Before each measurement, samples were stirred for 15 s and left to equilibrate for 5 s.

[Ir(ppy)(diFppy)(dtb-bpy)][PF_6] (2). 4,4′-Di-*tert*-butyl-2,2′-bipyridine (152 mg, 0.56 mmol) was added to a solution of **1** (147 mg, 0.14 mmol) in dichloromethane (20 mL) and methanol (5 mL). The mixture was refluxed overnight. After cooling to room temperature, KPF_6 (200 mg) was added as a solid and the dichloromethane (DCM) was removed under vacuum. Deionized water (5 mL) was added to the methanol and the suspension stirred for 20 min at room temperature. The solid was filtered, washed with water, and dried. **2** was obtained as a bright yellow solid (237 mg, yield 88%). ^{1}H NMR ($CDCl_3$, 400 MHz): δ 8.43 (dd, 2H, J = 5.6, 2.0 Hz); 8.28 (d, 1H, J = 8.4 Hz); 7.93 (d, 1H, J = 7.2 Hz); 7.87 (d, 1H, J = 5.6 Hz); 7.82−7.77 (m, 3H); 7.70 (dd, 1H, J = 8.0, 1.2 Hz); 7.67 (ddd, 1H, J = 6.0, 1.6, 0.8 Hz); 7.60 (ddd, 1H, J = 5.6, 1.2, 0.8 Hz); 7.46 (dd, 1H, J = 5.6, 1.6 Hz); 7.39 (dd, 1H, J = 6.0, 2.0 Hz); 7.17−7.11 (m, 2H); 7.08 (dt, 1H, J = 8.0, 1.2 Hz); 6.95 (dt, 1H, J = 7.2, 1.2 Hz); 6.51 (ddd, 1H, J = 12.8, 9.2, 2.4 Hz); 6.25 (dd, 1H, J = 7.6, 0.8 Hz); 5.76 (dd, 1H, J = 8.4, 2.4 Hz); 1.47 (s, 9H); 1.45 (s, 9H). ESI-TOF HRMS: $[M\text{-}PF_6]^+$ m/z: calcd.: 805.2697; found: 805.2814. Anal. Calcd. for $C_{40}H_{38}F_8IrN_4P$: C, 50.57; H, 4.03; N, 5.90. Found: C, 50.35; H, 3.76; N, 5.79.

[Ir(ppy)$_2$(dtb-bpy)][PF_6] (3). 4,4′-Di-*tert*-butyl-2,2′-bipyridine (112 mg, 0.41 mmol) was added to a solution of $[(ppy)_2IrCl]_2$ dimer (200 mg, 0.18 mmol) in DCM (40 mL) and methanol (5 mL). The mixture was refluxed overnight under nitrogen. After cooling to room temperature, KPF_6 (200 mg) was added as a solid and the DCM was removed under vacuum. Deionized water (5 mL) was added to the methanol and the suspension was stirred for 20 min at room temperature. The solid was filtered and washed with water and methanol. The solid then was dissolved in DCM and precipitated in diethylether. The crystals were collected, affording **3** as a bright yellow solid (303 mg, yield 90%). ^{1}H NMR ($CDCl_3$, 400 MHz): δ 8.35 (d, 2H, J = 1.8 Hz); 7.86 (broad d, 2H, J = 8.0 Hz); 7.80 (d, 2H, J = 5.8 Hz); 7.72 (dt, 2H, J = 8.0, 1.5 Hz); 7.39 (broad d, 2H, J = 7.0 Hz); 7.58 (broad d, 2H, J = 5.6 Hz); 7.36 (dd, 2H, J = 5.8, 1.9 Hz); 7.06 (ddd, 2H, J = 7.5, 6.0, 1.2 Hz); 6.98 (dt, 2H, J = 7.5, 1.0 Hz); 6.87 (dt, 2H, J = 7.5, 1.2 Hz); 6.27 (d, 2H, J = 7.5 Hz); 1.41 (s, 18H). ESI-TOF HRMS: $[M\text{-}PF_6]^+$ m/z: calcd.: 769.2885; found: 769.2870. Anal. Calcd. for $C_{40}H_{40}F_6IrN_4P$: C, 52.57; H, 4.41; N, 6.13. Found: C, 52.28; H, 4.24; N, 6.26.

[Ir(diFppy)$_2$(dtb-bpy)][PF_6] (4). 4,4′-Di-*tert*-butyl-2,2′-bipyridine (99 mg, 0.36 mmol) was added to a solution of $[(diFppy)_2IrCl]_2$ dimer (200 mg, 0.16 mmol) in DCM (40 mL) and methanol (5 mL). The mixture was refluxed overnight under nitrogen. After cooling to room temperature, KPF_6 (200 mg) was added as solid and the DCM was removed under vacuum. Deionized water (5 mL) was added to the methanol and the suspension was stirred for 20 min at room temperature. The solid was filtered and washed with water and methanol. The solid then was dissolved in DCM and precipitated in diethylether. The crystals were collected affording **4** as a pale yellow solid (269 mg, yield 83%). ^{1}H NMR ($CDCl_3$, 400 MHz): δ 8.41 (d, 2H, J = 1.8 Hz); 8.26 (broad d, 2H, J = 8.5 Hz); 7.77 (m, 4H); 7.59 (m, 2H, J = 5.0, 0.7 Hz); 7.41 (dd, 2H, J = 5.8, 1.8 Hz); 7.12 (ddd, 2H, J = 7.5, 5.8, 1.2 Hz); 7.52 (ddd, 2H, J = 12.4, 9.2, 2.3 Hz); 5.65 (dd, 2H, J = 8.5, 2.3 Hz); 1.42 (s, 18H). ESI-TOF HRMS: $[M\text{-}PF_6]^+$ m/z: calcd.: 841.2508; found: 841.2507. Anal. Calcd. for $C_{40}H_{36}F_{10}IrN_4P$: C, 48.73; H, 3.68; N, 5.68. Found: C, 48.75; H, 3.62; N, 5.62.

Theoretical Calculations. Density functional theory (DFT) calculations were carried out with the A.02 revision of the Gaussian 09 program package,[30] using Becke's three-parameter B3LYP exchange-correlation functional,[31,32] together with the 6-31G** basis set for C, H, F, and N,[33] and the "double-ζ" quality LANL2DZ basis set for the Ir element.[34] The geometries of the singlet ground state (S_0) and the lowest-energy triplet states were fully optimized without imposing any symmetry restriction. The geometries of the triplet states were calculated at the spin-unrestricted UB3LYP level with a spin multiplicity of 3. All the calculations were performed in the presence of the solvent (acetonitrile). Solvent effects were considered within the self-consistent reaction field (SCRF) theory using the SMD keyword that performs a polarized continuum model (PCM)[35−37] calculation using the solvation model of Thrular et al.[38] The SMD solvation model is based on the polarized continuous quantum chemical charge density of the solute (the "D" in the name stands for "density"). Time-dependent DFT (TD-DFT) calculations of the lowest-lying 20 triplets were performed in the presence of the solvent for complexes **2**, **3**, and **4** at the minimum-energy geometry optimized for the ground state (S_0).

Device Preparation and Characterization. Poly(3,4-ethylene dioxythiophene):polystyrene sulfonate (PEDOT:PSS) was purchased from Hereaus, and the solvents used were obtained from Aldrich. Indium tin oxide (ITO)-coated glass plates (15 Ω $\square^{-1}$) were patterned using conventional photolithography (obtained from Naranjosubstrates, www.naranjosubstrates.com). The substrates were extensively cleaned using sonication in subsequently water-soap, water, and 2-propanol baths. After drying, the substrates were placed in a UV-ozone cleaner (Jelight 42-220) for 20 min.

The electroluminescent devices were prepared as follows. Transparent thin films of complex **2** with the ionic liquid (1-butyl-3-methylimidazolium hexafluorophosphate) in a molar ratio of 4:1 were obtained by spinning from acetonitrile solutions using concentrations of 20 mg mL^{-1} at 1000 rpm for 20 s. The resulting films had a thickness of 80 nm. Prior to the deposition of the emitting layer, a 90-nm layer of PEDOT:PSS was deposited to increase the device preparation yield. The thickness of the films was determined using an Ambios XP1 profilometer. After spinning the organic layers, the samples were transferred to an inert atmosphere glovebox (<0.1 ppm O_2 and H_2O, MBraun) and dried on a hot plate at 100 °C for 1 h. Aluminum metal electrodes (70 nm) were thermally evaporated using a shadow mask under a vacuum ($<1 \times 10^{-6}$ mbar) using an Edwards Auto500 evaporator integrated into an inert atmosphere glovebox. Lifetime data were obtained by applying pulsed currents and monitoring the voltage and, simultaneously, the luminance by a True Color Sensor MAZeT (MTCSICT Sensor), using a Lifetime Test System designed by BoTEST (Botest OLT OLED Lifetime-Test System).

RESULTS AND DISCUSSION

Synthesis. The pure heteroleptic chloro-bridged iridium dimer **1** was prepared following our previously reported procedure.[28] We briefly recall this unusual synthetic procedure. The iridium(I) complex $[Ir(COD)(\mu\text{-}Cl)]_2$ (where COD =

dx.doi.org/10.1021/cm3011716 | Chem. Mater. 2012, 24, 1896−1903

1,5-cyclooctadiene) was reacted with 2 equiv of ppy and diFppy in 2-ethoxyethanol for 3 h. This resulted in a mixture of chloro-bridged iridium dimers, $[Ir_2(ppy)_{4-n}(diFppy)_n(\mu\text{-}Cl)_2]$ (n = 0–4). The mixture was reacted with acetylacetone and a base to obtain a mixture of heteroleptic mononuclear complexes, from which the complex [Ir(ppy)(diFppy)(acac)] can be isolated in good yield. Finally, the reaction of [Ir(ppy)(diFppy)(acac)] with hydrochloric acid (HCl) resulted in cleavage of the acac ancillary ligand and formation of the pure dimer **1**, $[Ir(ppy)(diFppy)(\mu\text{-}Cl)_2Ir(ppy)(diFppy)]$. This is the key step as the availability of the pure heteroleptic dimer allows for preparing new tris-heteroleptic complexes with high yields and without tedious purification methods. Accordingly, complex **2** was prepared using methods similar to those for other $[Ir(C^\wedge N)_2L]^+$ complexes by reacting **1** with 2 equiv of 4,4′-di-*tert*-butyl-2,2′-bipyridine in refluxing CH_2Cl_2/MeOH (4:1 v/v), followed by the addition of an excess of ammonium hexafluorophosphate (Scheme 1). Complexes **3** and **4** (Scheme 2) were prepared according to the literature methods,[9,27] to be able to compare exactly the photophysical properties and the performance in LECs. Details concerning the synthesis and the characterization of complexes **2**, **3**, and **4** can be found in the Experimental Section.

Scheme 1. Complex 2 is Formed by Reacting 1 with 2 equiv of 4,4′-Di-*tert*-butyl-2,2′-bipyridine in Refluxing CH_2Cl_2/MeOH (4:1 v/v), Followed by the Addition of an Excess of Ammonium Hexafluorophosphate

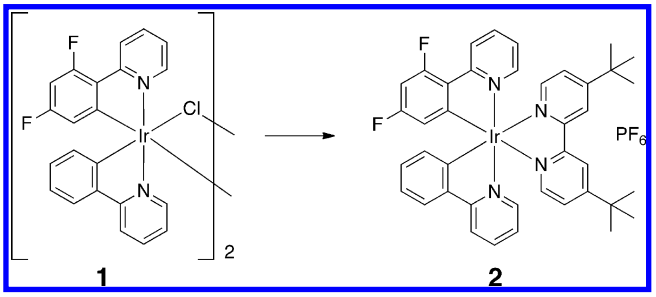

Scheme 2. Chemical Structures of Complexes 3 and 4

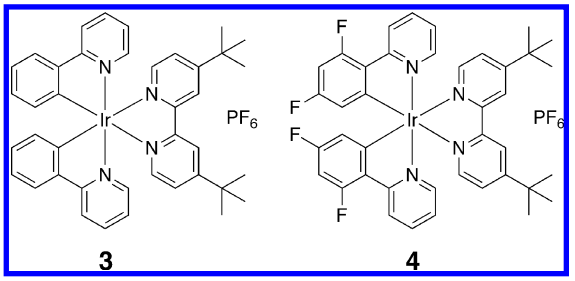

Photophysical and Electrochemical Studies. The photophysical and electrochemical properties of the tris-heteroleptic complex **2** are studied and compared with the bis-heteroleptic complexes **3** and **4** (see Table 1). The emission spectra of the complexes were recorded using an excitation wavelength of 420 nm in acetonitrile at room temperature and in CH_2Cl_2 glass at 77 K. Strong, broad, and nonstructured emissions with maxima at 588, 555, and 524 nm were observed at room temperature for **3**, **2**, and **4**, respectively (see Figure 1).

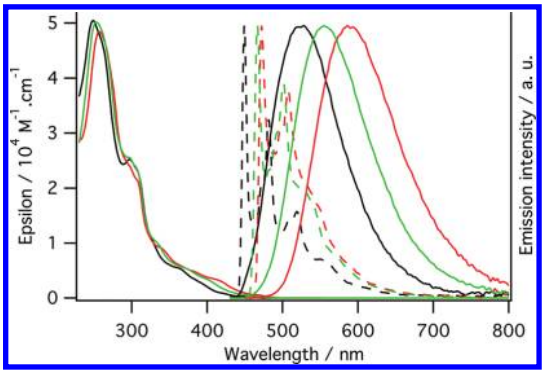

Figure 1. Absorption and emission spectra of **2** (green), **3** (red), and **4** (black). Solid lines represent data obtained in acetonitrile at room temperature, and dotted lines represent data obtained in CH_2Cl_2 at 77 K.

At 77 K, the spectra in CH_2Cl_2 become highly structured with emission maxima at 472, 466, and 449 nm for **3**, **2**, and **4**, respectively. The unstructured and broad emission band is typical of complexes containing a combination of orthometalating and neutral diimine ligands, and the significant rigidochromic effect on going to low temperature suggests a strong metal-to-ligand charge-transfer (MLCT) character of the emissive state at room temperature.[39,40] As for the emission maximum, the lifetime of the excited state (τ = 0.99 μs), and the photoluminescence quantum yield (Φ_{PL} = 0.59) of **2**, lie between the values recorded for **3** (τ = 0.55 μs and Φ_{PL} = 0.23) and **4** (τ = 1.25 μs and Φ_{PL} = 0.71). Assuming a unitary intersystem crossing, one can calculate the radiative and nonradiative constants (k_r and k_{nr}, respectively). It shows that the complexes follow the energy gap law as $\ln(k_{nr})$ decreases linearly with the energy of the emission maxima.

The electrochemical potentials have been measured in acetonitrile for the three charged complexes and are reported vs ferrocenium/ferrocene in Table 1. The redox potentials measured for all three complexes are quasi-reversible and both the oxidation and reduction potentials of **2** are close to the

Table 1. Photophysical and Electrochemical Properties in MeCN Solution of 2, 3, and 4

	Emission						Redox Potentials[e]	
	At 298 K[a]					At 77 K[d]		
	λ_{max} (nm)	τ[b] (μs)	Φ_{PL}	k_r[c] ($\times 10^5$ s^{-1})	k_{nr}[c] ($\times 10^5$ s^{-1})	λ_{max} (nm)	E_{ox} (V)	E_{red} (V)
3	588	0.55	0.23	4.17	14.0	472	0.85	−1.87
2	555	0.99	0.59	5.99	4.16	466	1.00	−1.83
4	524	1.25	0.71	5.68	2.32	449	1.17	−1.80

[a]Argon-saturated 10^{-5} M solution, λ_{exc} = 420 nm. [b]Nanoled excitation at 406 nm. [c]Assuming unitary intersystem crossing, $k_r = \Phi/\tau$ and $k_{nr} = (1 - \Phi)/\tau$. [d]In CH_2Cl_2. [e]vs Fc^+/Fc.

dx.doi.org/10.1021/cm3011716 | Chem. Mater. 2012, 24, 1896–1903

average of the two bis-heteroleptic complexes. This points to similar HOMO and LUMO localizations on both the phenyl ring and the iridium center and on the bipyridine, respectively, as observed for most of the bis-heteroleptic cyclometalated iridium ionic complexes with an N^N ancillary ligand. This view is further supported by DFT calculations (see below).

Theoretical Calculations. To gain insight into the electronic and optical properties of **2**, DFT calculations were performed at the B3LYP/(6-31G**/LANL2DZ) level on the $[Ir(ppy)(diFppy)(dtb\text{-}bpy)]^+$ cation in acetonitrile solution (see the Experimental Section for full computational details). The molecular and electronic structures of the cations of complexes **3** and **4** were also investigated for comparison purposes.

Figure 2 displays the atomic orbital composition calculated for the highest-occupied and lowest-unoccupied molecular

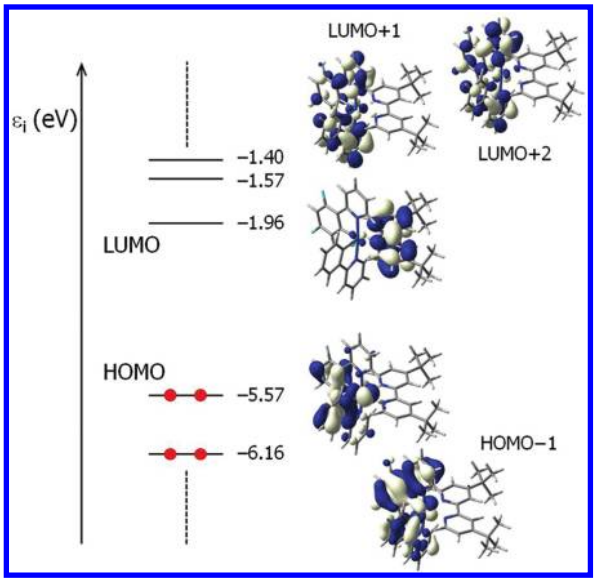

Figure 2. Schematic representation showing the electronic density contours (0.03 e $bohr^{-3}$) and energies calculated for the frontier molecular orbitals of complex **2**.

orbitals of **2**. As already reported for analogous bis-heteroleptic cyclometalated Ir-iTMCs,[10,41,42] the HOMO is composed of a mixture of Ir(III) d_π orbitals (t_{2g}) and phenyl π orbitals of the cyclometalating ligands and the LUMO corresponds to the π^* LUMO of the ancillary bpy ligand. It is important to stress that, in contrast to what is computed for **3** and **4**, for which the two cyclometalating ligands equally contribute to the HOMO, the contribution of the ppy ligand to this orbital in complex **2** is significantly larger than that of the diFppy. The phenyl ring of the diFppy ligand is stabilized by the electron-withdrawing effect of the F atoms, and this ligand contributes to a larger extent to the HOMO−1, calculated 0.59 eV below the HOMO (see Figure 2). The stabilizing effect of the F atoms affects the HOMO and this orbital is calculated at −5.57 eV, which exactly corresponds to the average of the energies computed for the HOMO of **3** (−5.43 eV) and **4** (−5.72 eV). It also causes a widening of the HOMO−LUMO energy gap in passing from **3** (3.45 eV) to **2** (3.61 eV) and to **4** (3.73 eV), since the energy of the LUMO remains mostly unaffected (see Figure 3). This widening agrees with the increase of 0.25 V measured experimentally for the electrochemical gap in going from **3**

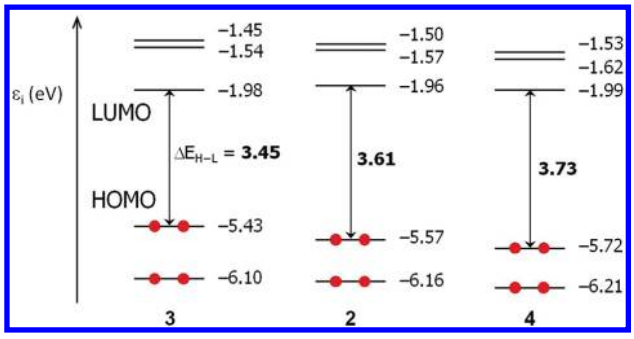

Figure 3. Energy diagram for the frontier molecular orbitals of complexes **3** (left), **2** (center), and **4** (right).

(2.72 V) to **4** (2.97 V), and is consistent with the blue shift observed in the photoluminescence spectra (see Table 1).

The LUMO+1 and LUMO+2 of **2** are localized over the ppy and diFppy ligands and are calculated as being very close in energy: 0.39 and 0.46 eV above the LUMO (−1.96 eV), respectively (see Figure 2). This suggests that the lowest-energy triplet state originates from the HOMO→LUMO excitation giving rise to an electron transfer from the Ir-phenyl environment to the diimino ligand. To investigate the nature of the emitting excited state, the low-lying triplet states of complexes **2**, **3**, and **4** were calculated at the optimized geometries of the ground state (S_0) using the time-dependent DFT (TD-DFT) approach. Table 2 summarizes the vertical excitation energies calculated for the first four triplets, together with their molecular orbital description and electronic nature. TD-DFT calculations predict the three first triplet states at close energies: 2.82 (T_1), 2.89 (T_2), and 2.90 eV (T_3) above the ground state for complex **2**. Surprisingly, the T_1 state is mainly defined by transitions from the HOMO to the LUMO +1 (40%) and LUMO+2 (21%), and it is described as a ligand-centered (^{3}LC) triplet, since both the HOMO and the LUMO +1 and LUMO+2 involve the C^N ligands, with some metal-to-ligand charge transfer (^{3}MLCT) character, because of the participation of the Ir core in the HOMO (Figure 2). The T_2 state lies 0.07 eV above T_1 and mainly results from the HOMO→LUMO excitation (90%). It corresponds to a mixture of metal-to-ligand and ligand-to-ligand charge transfer (^{3}MLCT/^{3}LLCT) character. Finally, T_3 is a combination of transitions from the HOMO−1 and HOMO to the LUMO+1 and LUMO+2, and has a ^{3}LC nature with some ^{3}MLCT character. A similar energy ordering is found for the three lowest-energy triplets of complex **4** (see Table 2), for which the HOMO→LUMO ^{3}MLCT/^{3}LLCT triplet corresponds to T_3 and is calculated 0.09 eV above T_1. For complex **3**, the HOMO→LUMO triplet is the lowest triplet and it is also very close in energy to the ^{3}LC/^{3}MLCT triplets T_2 and T_3 (see Table 2).

The lowest triplet states of complex **2** were further examined by optimizing their geometries using the spin-unrestricted DFT approach (see Table S1 in the Supporting Information). After full-geometry relaxation, the T_1, T_2, and T_3 states are calculated 2.68, 2.62, and 2.76 eV above S_0 (adiabatic energy differences), respectively, and T_2 becomes the most-stable triplet (Figure 4). The unpaired-electron spin-density distribution computed for the optimized geometry of T_2 (Ir, 0.50e; ppy, 0.32e; diFppy, 0.16e; dtb-bpy, 1.02e) confirms the mixed ^{3}MLCT/^{3}LLCT character of this state and illustrates the higher contribution of the ppy ligand, compared with the diFppy ligand, to the

dx.doi.org/10.1021/cm3011716 | Chem. Mater. 2012, 24, 1896−1903

Table 2. Lowest Triplet Excited States Calculated at the TD-DFT B3LYP/(6-31G+LANL2DZ) Level for Complexes 2, 3, and 4 in Acetonitrile Solution[a]**

state	E (eV)	monoexcitations	nature	description
Complex 2				
T_1	2.82	H → L+1 (40)	$d_\pi(Ir) + \pi_{ppy} \rightarrow \pi^*_{ppy}$	^{3}LC/^{3}MLCT
		H → L+2 (21)	$d_\pi(Ir) + \pi_{ppy} \rightarrow \pi^*_{ppy}$	
T_2	2.89	H → L (91)	$d_\pi(Ir) + \pi_{ppy} \rightarrow \pi^*_{bpy}$	^{3}MLCT/^{3}LLCT
T_3	2.90	H−1→ L+1 (27)	$d_\pi(Ir) + \pi_{ppy} \rightarrow \pi^*_{ppy}$	^{3}LC/^{3}MLCT
		H → L+1 (17)	$d_\pi(Ir) + \pi_{ppy} \rightarrow \pi^*_{ppy}$	
		H → L+2 (29)	$d_\pi(Ir) + \pi_{ppy} \rightarrow \pi^*_{ppy}$	
T_4	3.10	H-6 → L+1 (48)	$\pi_{bpy} \rightarrow \pi^*_{ppy}$	^{3}LLCT
		H-2 → L (17)	$d_\pi(Ir) + \pi_{ppy} \rightarrow \pi^*_{bpy}$	
Complex 3				
T_1	2.73	H→ L (96)	$d_\pi(Ir) + \pi_{ppy} \rightarrow \pi^*_{bpy}$	^{3}MLCT/^{3}LLCT
T_2	2.77	H−1 → L+2 (15)	$d_\pi(Ir) + \pi_{ppy} \rightarrow \pi^*_{ppy}$	^{3}LC/^{3}MLCT
		H → L+1 (67)	$d_\pi(Ir) + \pi_{ppy} \rightarrow \pi^*_{ppy}$	
T_3	2.82	H−1 → L+1 (24)	$d_\pi(Ir) + \pi_{ppy} \rightarrow \pi^*_{ppy}$	^{3}LC/^{3}MLCT
		H → L+2 (55)	$d_\pi(Ir) + \pi_{ppy} \rightarrow \pi^*_{ppy}$	
T_4	3.03	H−4 → L (43)	$d_\pi(Ir) + \pi_{ppy} \rightarrow \pi^*_{bpy}$	^{3}MLCT/^{3}LLCT
		H−2 → L (0.31)	$d_\pi(Ir) + \pi_{ppy} \rightarrow \pi^*_{bpy}$	
Complex 4				
T_1	2.90	H−1 → L+2 (23)	$d_\pi(Ir) + \pi_{ppy} \rightarrow \pi^*_{ppy}$	^{3}LC/^{3}MLCT
		H → L+1 (52)	$d_\pi(Ir) + \pi_{ppy} \rightarrow \pi^*_{ppy}$	
T_2	2.93	H−1 → L+1 (32)	$d_\pi(Ir) + \pi_{ppy} \rightarrow \pi^*_{ppy}$	^{3}LC/^{3}MLCT
		H → L+2 (40)	$d_\pi(Ir) + \pi_{ppy} \rightarrow \pi^*_{ppy}$	
T_3	2.99	H→ L (79)	$d_\pi(Ir) + \pi_{ppy} \rightarrow \pi^*_{bpy}$	^{3}MLCT/^{3}LLCT
T_4	3.12	H−6 → L (43)	$\pi_{bpy} \rightarrow \pi^*_{bpy}$	^{3}LC
		H → L (19)	$d_\pi(Ir) + \pi_{ppy} \rightarrow \pi^*_{bpy}$	

[a]Vertical excitation energies (E), dominant monoexcitations with contributions (within parentheses) of >15%, the nature of the electronic transition, and the description of the excited state are summarized.

electron transfer that takes place in this state to the diimine ligand. The different participation of the two cyclometalated ligands is also evidenced by the asymmetric contraction of the coordination sphere obtained for T_2. Compared with S_0, the Ir−C(ppy) bond shortens by 0.039 Å, whereas the Ir−C(diFppy) bond decreases by only 0.006 Å (see Table S1 in the Supporting Information). In complexes **3** and **4**, the Ir−C(ppy) and Ir−C(diFppy) bonds symmetrically shorten by 0.026 and 0.020 Å, respectively. The presence of two different cyclometalated ligands in complex **2** also induces a significant asymmetry of the Ir−N distances (2.199 and 2.184 Å) on the 4,4′-di-*tert*-butyl-2,2′-bipyridine ancillary ligand. The spin densities calculated for T_1 (Ir, 0.26e; ppy, 1.72e; diFppy, 0.02e; dtb-bpy, 0.00e) and T_3 (Ir, 0.28e; ppy, 0.04e; diFppy, 1.67e; dtb-bpy, 0.01e) of complex **2** confirm the dominant ^{3}LC nature of these states and reveals that they involve a different C^N ligand, T_1 spreads over the ppy and T_2 over the diFppy (see Figure 4). The spin-density distributions calculated for the lowest ^{3}MLCT/^{3}LLCT (HOMO→LUMO) and ^{3}LC triplets of complexes **3** and **4** are illustrated in Figures S1 and S2 in the Supporting Information.

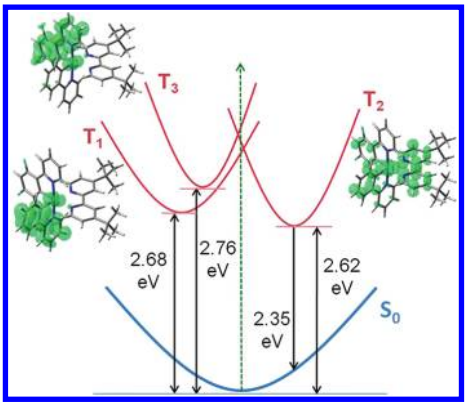

Figure 4. Schematic representation of the ground state (S_0, blue curve) and the first three triplet states (T_1, T_2, and T_3, red curves) computed for **2** with their respective spin-density distributions (0.003 e bohr^{-3}).

Calculations therefore predict that emission in complex **2** occurs from the T_2 ^{3}MLCT/^{3}LLCT triplet that implies an electron transfer from the Ir−ppy environment to the diimine ligand. The CT nature of the emitting triplet is in agreement with the broad and unstructured aspect of the emission band observed at 2.23 eV (555 nm). To estimate the emission energy, the vertical energy difference between the emitting triplet and S_0 was determined by performing a single-point calculation of S_0 at the optimized minimum-energy geometry of the triplet. Calculations lead to a vertical emission of 2.35 eV (528 nm) slightly overestimating the experimental energy. The emission energy obtained for **2** is intermediate between those calculated for the bis-heteroleptic complexes **3** (2.24 eV, 553 nm) and **4** (2.50 eV, 496 nm), in good agreement with the experiment (**3**, 2.11 eV; **2**, 2.23 eV; **4**, 2.37 eV; see Table 1).

Light-Emitting Devices. Finally, to explore the electroluminescence properties of the complexes, simple two-layer LECs were prepared by spin coating a thin layer (90 nm) of poly(3,4-ethylenedioxythiophene):poly(styrene sulfonate) (PEDOT:PSS) on top of a patterned indium tin oxide (ITO)-coated glass substrate, followed by an active layer (80 nm) consisting of complex **2** mixed with the ionic liquid (IL) 1-butyl-3-methylimidazolium hexafluorophosphate [BMIM$^+$:PF$_6^-$] at a molar ratio of 4:1, which was added to reduce the turn-on time. A 70-nm aluminum layer was used as the top electrode contact. Similar device configurations were prepared using complexes **3** and **4** for comparison purposes. More details concerning the device preparation can be found in the Experimental Section.

The LECs were driven using a recently reported method of a pulsed current with an average current density of 100 A m^{-2} using a block wave at a frequency of 1000 Hz and a duty cycle of 50%.[8] These driving conditions were selected because current driving leads to fast turn-on times and pulsed driving stabilizes the doped regions leading to increased lifetimes. More importantly, the lifetimes observed with this driving method are

dx.doi.org/10.1021/cm3011716 | Chem. Mater. 2012, 24, 1896−1903

linked to intrinsic instabilities of the device and complex used therein.

The first important observation from the devices is their EL spectrum (Figure 5). It coincides with the photoluminescence

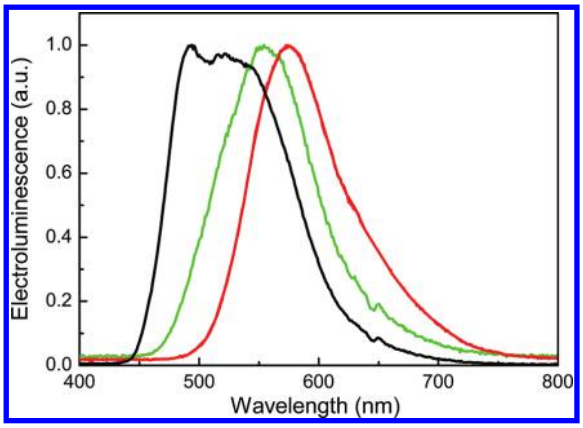

Figure 5. Electroluminescent spectra for ITO/PEDOT:PSS/iTMC:IL(4:1)/Al LEC devices driven at a pulsed current with an average current density of 100 A m^{-2}, using a block wave at a frequency of 1000 Hz and a duty cycle of 50%, where iTMC is **2** (green), **3** (red), and **4** (black).

spectrum recorded in solution for complexes **2** and **3**. In contrast, the EL spectrum of LECs using complex **4** is slightly different, because it is significantly broadened and two maxima can be identified (493 and 516 nm). This is a first hint toward the instability of complex **4** under these conditions. The EL spectrum of the LECs using the tris-heteroleptic complex lies between those of the LECs based on the two bis-heteroleptic equivalents, which confirms the photophysical trends and quantum-chemical results presented above.

The luminance and average voltage versus operation time are represented in Figure 6 for the three LECs. All three devices reach their maximum luminance within 30 min as a result of the (pulsed) current driving. The average voltage required to sustain the 100 A m^{-2} current density drops rapidly over the first minutes, after which it remains almost constant. This can be understood in view of the operational mechanism of LECs, which requires ionic motion to reduce the electronic injection

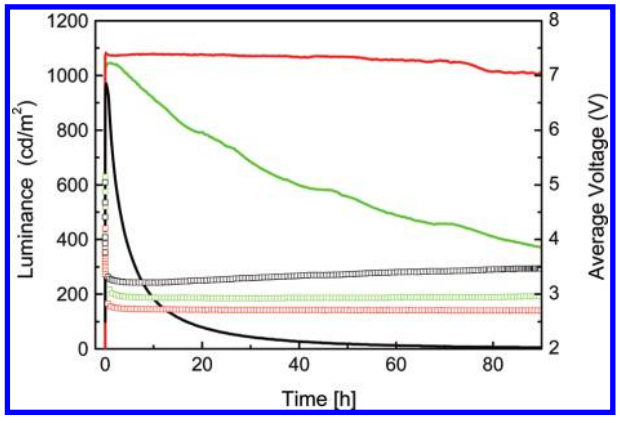

Figure 6. Luminance (line) and average voltage (open squares) for ITO/PEDOT:PSS/iTMC:IL(4:1)/Al LEC devices driven at a pulsed current with an average current density of 100 A m^{-2}, using a block wave at a frequency of 1000 Hz and a duty cycle of 50%, where iTMC is **2** (green), **3** (red), and **4** (black).

barriers. Upon biasing the device, the initial barriers for electrons and holes are large, and, therefore, a relatively high voltage is required to maintain the current density at 100 A m^{-2}. However, this high voltage leads to more rapid ion movement and, subsequently, to the reduction of the electronic injection barriers. As this occurs, the voltage needed drops gradually to reach the value that is related to the bulk transport through the iTMC layer. It is interesting to note that the voltage decreases in going from LECs using complex **4**, to **2**, and to **3**, which might be related to the electron and hole mobility of the different iTMC-based films.

The maximum luminance drops for LECs using complexes **2** and **4**, whereas it is maintained for approximately one day in the case of LECs based on complex **3** (see Figure 6). The luminance of LECs with complex **4** decreases the fastest, indicating low stability. The average driving voltage needed to maintain the 100 A m^{-2} reaches a minimum, after which it remains constant for LECs based on complexes **2** and **3**, whereas it slowly increases for the LEC using complex **4**. The increase in driving voltage is a typical sign of permanent degradation of the active materials. The key performance parameters are listed in Table 3.

Table 3. Performance of LEC Devices Driven at a Pulsed Current with an Average Current Density of 100 A m^{-2}, Using a Block Wave at a Frequency of 1000 Hz and a Duty Cycle of 50%

	t_{on}[a] (s)	luminance$_{max}$ (cd m^{-2})	$t_{1/2}$[b] (h)	efficacy (cd A^{-1})	power efficiency (lm W^{-1})	external quantum efficiency, EQE (%)
3	9.0	1083	370	10.8	6.1	3.49
2	4.5	1046	55	10.4	5.3	2.99
4	5.5	970	3.3	9.7	4.3	2.83

[a]Defined as the time needed to reach 100 cd m^{-2}. [b]Defined as the time needed to reach half of the maximum luminance.

There is a small difference in the device efficiency, best expressed as the external quantum efficiency (EQE), because this is independent of the emission wavelength. Noteworthy, the EQE of the devices shows the inverse order (**3** > **2** > **4**), compared with the Φ_{PL} values of the complexes in solution (**4** > **2** > **3**). This might be explained by an increased balance of the hole and electron mobility in films of complexes **3** and **2**. Balanced hole and electron mobilities in LECs lead to a recombination and exciton generation zone in the center of the device, less prone to the quenching effects of the *p*+ and *n*− doped zones at the interface with the electrodes.

The most striking difference between the three LECs, beside their emission color, is the lifetime, which is expressed as the time needed to reach 50% of the peak luminance ($t_{1/2}$). Because the peak luminance is similar in all devices, this figure of merit can be used to evaluate the stability. The lifetime decreases strongly in going from the device employing complex **3**, to that based on complexes **2** and **4**, respectively (see Figure 6). This indicates that the stability is directly related to the number of fluorine-containing ligands in the complex and that the decrease of the stability can be rationalized by the increasing number of fluorine substituents.

dx.doi.org/10.1021/cm3011716 | *Chem. Mater.* 2012, 24, 1896−1903

CONCLUSIONS

A light-emitting electrochemical cell (LEC) based on a tris-heteroleptic iridium complex shows very bright, efficient, and stable green electroluminescence. The ionic tris-heteroleptic iridium complex is prepared using a new and efficient synthetic procedure. The new complex is compared with its bis-heteroleptic analogs, using both photophysical and quantum chemical calculations, which show and rationalize that the redox and emission properties of the tris-heteroleptic complex are situated between the two bis-heteroleptic complexes. All three complexes were used to prepare LECs, and their electroluminescence spectra confirm that the tris-heteroleptic complex lies between its two bis-heteroleptic analogs. Therefore, tris-heteroleptic complexes provide the opportunity of fine-tuning the emission properties and bridging gaps between a series of bis-heteroleptic complexes. Interestingly, the stability of the LECs reduces as the number of fluorine-containing cyclometalating ligands increases.

ASSOCIATED CONTENT

Supporting Information

Additional theoretical data available as Supporting Information. This material is available free of charge via the Internet at http://pubs.acs.org.

AUTHOR INFORMATION

Corresponding Author

*E-mails: henk.bolink@uv.es (H.J.B.), e.baranoff@bham.ac.uk (E.B.).

Notes

The authors declare no competing financial interest.

ACKNOWLEDGMENTS

This work has been supported by the European Union (CELLO, Grant STRP 248043; https://www.cello-project.eu/) and the Spanish Ministry of Economy and Competitiveness (MINECO) (MAT2011-24594, CSD2007-00010, and CTQ2009-08790). D.T. and M.D. acknowledge the support of a FPU grant of the Spanish Ministry of Education, Culture, and Sport (MECD).

REFERENCES

(1) Pei, Q.; Yu, G.; Zhang, C.; Yang, Y.; Heeger, A. J. *Science* **1995**, *269*, 1086.
(2) Maness, K. M.; Terrill, R. H.; Meyer, T. J.; Murray, R. W.; Wightman, R. M. *J. Am. Chem. Soc.* **1996**, *118*, 10609.
(3) Slinker, J. D.; Rivnay, J.; Moskowitz, J. S.; Parker, J. B.; Bernhard, S.; Abruña, H. D.; Malliaras, G. G. *J. Mater. Chem.* **2007**, *17*, 2976.
(4) Sun, Q.; Li, Y.; Pei, Q. B. *J. Display Technol.* **2007**, *3*, 211.
(5) Hu, T.; He, L.; Duan, L.; Qiu, Y. *J. Mater. Chem* **2012**, *22*, 4206.
(6) Slinker, J. D.; DeFranco, J. A.; Jaquith, M. J.; Silveira, W. R.; Zhong, Y.; Moran-Mirabal, J. M.; Graighead, H. G.; Abruña, H. D.; Marohn, J. A.; Malliaras, G. G. *Nat. Mater.* **2007**, *6*, 894.
(7) Matyba, P.; Maturova, K.; Kemerink, M.; Robinson, N. D.; Edman, L. *Nat. Mater.* **2009**, *8*, 672.
(8) Tordera, D.; Meier, S.; Lenes, M.; Costa, R. D.; Orti, E.; Sarfert, W.; Bolink, H. J. *Adv. Mater.* **2011**, *24*, 897.
(9) Slinker, J. D.; Gorodetsky, A. A.; Lowry, M. S.; Wang, J.; Parker, S.; Rohl, R.; Bernhard, S.; Malliaras, G. G. *J. Am. Chem. Soc.* **2004**, *126*, 2763.
(10) Tamayo, A. B.; Garon, S.; Sajoto, T.; Djurovich, P. I.; Tsyba, I.; Bau, R.; Thompson, M. E. *Inorg. Chem.* **2005**, *44*, 8723.
(11) Bolink, H. J.; Cappelli, L.; Coronado, E.; Graetzel, M.; Ortí, E.; Costa, R. D.; Viruela, M.; Nazeeruddin, M. K. *J. Am. Chem. Soc.* **2006**, *128*, 14786.
(12) Su, H. C.; Fang, F. C.; Hwu, T. Y.; Hsieh, H. H.; Chen, H.; Lee, G.; Peng, S.; Wong, K. T.; Wu, C. C. *Adv. Funct. Mater.* **2007**, *17*, 1019.
(13) Bolink, H. J.; Coronado, E.; Costa, R. D.; Ortí, E.; Sessolo, M.; Graber, S.; Doyle, K.; Neuburger, M.; Housecroft, C. E.; Constable, E. C. *Adv. Mater.* **2008**, *20*, 3910.
(14) Graber, S.; Doyle, K.; Neuburger, M.; Housecroft, C. E.; Constable, E. C.; Costa, R. D.; Ortí, E.; Repetto, D.; Bolink, H. J. *J. Am. Chem. Soc.* **2008**, *130*, 14944.
(15) He, L.; Duan, L.; Qiao, J.; Wang, R.; Wei, P.; Wang, L.; Qiu, Y. *Adv. Funct. Mater.* **2008**, *18*, 2123.
(16) Zysman-Colman, E.; Slinker, J. D.; Parker, J. B.; Malliaras, G. G.; Bernhard, S. *Chem. Mater.* **2008**, *20*, 388.
(17) Rothe, C.; Chiang, C.; Jankus, V.; Abdullah, K.; Zeng, X.; Jitchati, R.; Batsanov, A. S.; Bryce, M. R.; Monkman, A. P. *Adv. Funct. Mater.* **2009**, *19*, 2038.
(18) Sun, L.; Galan, A.; Ladouceur, S.; Slinker, J. D.; Zysman-Colman, E. *J. Mater. Chem.* **2011**, *21*, 18083.
(19) Lowry, M. S.; Goldsmith, J. I.; Slinker, J. D.; Rohl, R.; Pascal, R. A.; Malliaras, G. G.; Bernhard, S. *Chem. Mater.* **2005**, *17*, 5712.
(20) Tamayo, A. B.; Garon, S.; Sajoto, T.; Djurovich, P. I.; Tsyba, I.; Bau, R.; Thompson, M. E. *Inorg. Chem.* **2005**, *44*, 8723.
(21) Bolink, H. J.; Cappelli, L.; Coronado, E.; Parham, A.; Stoessel, P. *Chem. Mater.* **2006**, *18*, 2778.
(22) Nazeeruddin, M. K.; Wegh, R. T.; Zhou, Z.; Klein, C.; Wang, Q.; De Angelis, F.; Fantacci, S.; Grätzel, M. *Inorg. Chem.* **2006**, *45*, 9245.
(23) Su, H. C.; Wu, C. C.; Fang, F. C.; Wong, K. T. *Appl. Phys. Lett.* **2006**, *89*, 261118.
(24) Costa, R. D.; Cespedes-Guirao, J.; Ortí, E.; Bolink, H. J.; Gierschner, J.; Fernandez-Lazaro, F.; Sastre-Santos, A. *Chem. Commun.* **2009**, *26*, 3886.
(25) He, L.; Qiao, J.; Duan, L.; Dong, G.; Zhang, D.; Wang, L.; Qiu, Y. *Adv. Funct. Mater.* **2009**, *19*, 2950.
(26) Rodriguez-Redondo, J. L.; Costa, R. D.; Ortí, E.; Sastre-Santos, A.; Bolink, H. J.; Fernandez-Lazaro, F. *Dalton Trans.* **2009**, 9787.
(27) Bolink, H. J.; Coronado, E.; Costa, R. D.; Lardiés, N.; Ortí, E. *Inorg. Chem.* **2008**, *47*, 9149.
(28) Baranoff, E.; Curchod, B. F. E.; Frey, J.; Scopelliti, R.; Kessler, F.; Tavernelli, I.; Rothlisberger, U.; Grätzel, M.; Nazeeruddin, M. K. *Inorg. Chem.* **2012**, *51*, 215.
(29) Shen, J.; Snook, R. D. *Chem. Phys. Lett.* **1989**, *155*, 583.
(30) Frisch, M. J.; Trucks, G. W.; Schlegel, H. B.; Scuseria, G. E.; Robb, M. A.; Cheeseman, J. R.; Scalmani, G.; Barone, V.; Mennucci, B.; Petersson, G. A.; Nakatsuji, H.; Caricato, M.; Li, X.; Hratchian, H. P.; Izmaylov, A. F.; Bloino, J.; Zheng, G.; Sonnenberg, J. L.; Hada, M.; Ehara, M.; Toyota, K.; Fukuda, R.; Hasegawa, J.; Ishida, M.; Nakajima, T.; Honda, Y.; Kitao, O.; Nakai, H.; Vreven, T.; Montgomery, J., J. A.; Peralta, J. E.; Ogliaro, F.; Bearpark, M.; Heyd, J. J.; Brothers, E.; Kudin, K. N.; Staroverov, V. N.; Kobayashi, R.; Normand, J.; Raghavachari, K.; Rendell, A.; Burant, J. C.; Iyengar, S. S.; Tomasi, J.; Cossi, M.; Rega, N.; Millam, J. M.; Klene, M.; Knox, J. E.; Cross, J. B.; Bakken, V.; Adamo, C.; Jaramillo, J.; Gomperts, R.; Stratmann, R. E.; Yazyev, O.; Austin, A. J.; Cammi, R.; Pomelli, C.; Ochterski, J. W.; Martin, R. L.; Morokuma, K.; Zakrzewski, V. G.; Voth, G. A.; Salvador, P.; Dannenberg, J. J.; Dapprich, S.; Daniels, A. D.; Farkas, Ö.; Foresman, J. B.; Ortiz, J. V.; Cioslowski, J.; Fox, D. J. *Gaussian 09, Revision A.02*; Gaussian, Inc.: Wallingford, CT, 2009.
(31) Lee, C. T.; Yang, W. T.; Parr, R. G. *Phys. Rev. B* **1988**, *37*, 785.
(32) Becke, A. D. *J. Chem. Phys.* **1993**, *98*, 5648.
(33) Francl, M. M.; Pietro, W. J.; Hehre, W. J.; Binkley, J. S.; Gordon, M. S.; Defrees, D. J.; Pople, J. A. *J. Chem. Phys.* **1982**, *77*, 3654.
(34) Hay, P. J.; Wadt, W. R. *J. Chem. Phys.* **1985**, *82*, 299.
(35) Tomasi, J.; Persico, M. *Chem. Rev.* **1994**, *94*, 2027.
(36) Cramer, C. S.; Truhlar, D. G. *Solvent Effects and Chemical Reactivity*; Kluwer: Dordrecht, The Netherlands, 1996.

(37) Tomasi, J.; Mennucci, B.; Cammi, R. *Chem. Rev.* **2005**, *105*, 2999.
(38) Marenich, A. V.; Cramer, C. J.; Truhlar, D. G. *J. Phys. Chem. B* **2009**, *113*, 6378.
(39) Bolink, H. J.; Cappelli, L.; Cheylan, S.; Coronado, E.; Costa, R. D.; Lardies, N.; Nazeeruddin, M. K.; Orti, E. *J. Mater. Chem.* **2007**, *17*, 5032.
(40) Tamayo, A. B.; Alleyne, B. D.; Djurovich, P. I.; Lamansky, S.; Tsyba, I.; Ho, N. N.; Bau, R.; Thompson, M. E. *J. Am. Chem. Soc.* **2003**, *125*, 7377.
(41) De Angelis, F.; Fantacci, S.; Evans, N.; Klein, C.; Zakeeruddin, S. M.; Moser, J. E.; Kalyanasundaram, K.; Bolink, H. J.; Graetzel, M.; Nazeeruddin, M. K. *Inorg. Chem.* **2007**, *46*, 5989.
(42) Costa, R. D.; Ortí, E.; Bolink, H. J.; Graber, S.; Schaffner, S.; Neuburger, M.; Housecroft, C. E.; Constable, E. C. *Adv. Funct. Mater.* **2009**, *19*, 3456.